Arcs from a Universal Dark-Matter Halo Profile

Matthias Bartelmann

Max-Planck-Institut für Astrophysik, P.O. Box 1523, D–85740 Garching, Germany

Abstract. Navarro, Frenk, & White have recently found numerically that the density profile of dark-matter halos can be described by a universal two-parameter function over a broad range of halo masses. The profile is singular, approaching the halo center with $\rho \propto r^{-1}$. It had been argued previously that radially distorted, gravitationally lensed images of background sources in galaxy clusters, so-called radial arcs, required a flat core in the cluster density profile. Such radial arcs have so far been detected in two galaxy clusters, in apparent contradiction with a singular density profile. I show here that the profile suggested by Navarro et al. can produce radial arcs despite its central singularity, and describe how the two parameters of the profile can be determined in clusters where radial and tangential arcs are observed. I then apply this analysis to the two clusters where radial arcs were detected. In both cases, the redshifts of the radial arcs are yet unknown, hence definitive conclusions on the profile parameters cannot yet be drawn. Numerically determined values for the parameters of cluster-sized halos can, however, be used to predict the range of the unknown arc redshifts, thus providing a direct observational test for the proposed density profile. A potential difficulty with the profile is that the radial magnification of tangential arcs is large, hence tangential arcs should be thick or their sources should be very thin in the radial direction.

1. Introduction

Navarro, Frenk, & White (1995a,b) have recently found that the density profile of dark-matter halos numerically simulated in the framework of the standard CDM cosmogony can very well be described by the radial function

$$\rho(x) = \frac{\rho_\mathrm{s}}{x(1+x)^2} \;, \tag{1.1}$$

within the broad halo mass range $3\times10^{11} \lesssim M_{200}/M_\odot \lesssim 3\times10^{15}$. Particular care was taken to investigate and rule out numerical artifacts of the simulations. The radial coordinate x is the radius in units of a scale radius r_s, $x \equiv r/r_\mathrm{s}$. The profile flattens towards the halo center but does not have a flat core. Although Navarro et al. restricted their original study to the standard CDM cosmogony, it has turned out that (1.1) provides excellent fits also to halos formed in other cosmogonies or from density fluctuations described by a variety of power-law perturbation spectra (Cole & Lacey 1995). It therefore appears that the profile

(1.1) can be considered as a universal two-parameter function describing the structure of dark-matter halos, independent of the size of the halos and the environment in which they form.

On the other hand, it has frequently been stated before that the occurrence of so-called radial arcs in galaxy clusters required the density to be constant approximately out to the distance of the radial arc from the center of the cluster, and core radii have been derived from the positions of radial arcs (e.g. Mellier, Fort, & Kneib 1993; Smail et al. 1995). This statement was mainly supported by one particular choice for the density profile of clusters, the non-singular isothermal profile, for which the location of radial arcs indeed provides an estimate for the core radius. Noting that profiles with a flat core may be poor choices for real clusters, Miralda-Escudé (1995) has recently studied a variety of singular and non-singular density profiles with regard to the location of radial arcs and their counter-images. Radial arcs are gravitationally distorted images of galaxies in the background of clusters which are radially elongated rather than tangentially as most giant luminous arcs are. They are much less numerous than (tangential) giant luminous arcs. So far, only in the clusters MS 2137 (Fort et al. 1992) and Abell 370 (Smail et al. 1995) have radial arcs been reported, but several more have been observed (J.-P. Kneib 1996, private communication). In both cases, the separation of the radial arcs from the cluster centers are such that they were interpreted in terms of cluster core sizes on the order of $20\,h^{-1}$kpc, where the Hubble constant is $H_0 = 100\,h$ km s^{-1} Mpc^{-1}. The implications of the radial arc in MS 2137 for a variety of mass profiles have also been discussed by Miralda-Escudé (1995).

I show in Sect. 2 of this paper that the singular profile (1.1) necessarily produces a radial critical curve. I also show that the existence of the radial critical curve is stable against perturbing the lens with an external shear field as long as the shear is small, $|\gamma| < 1$. I describe how the two parameters of the profile (1.1) can be measured in clusters where radial and tangential arcs are observed. In Sect. 3, I analyze the two cases of radial arcs so far detected, and in Sect. 4 I summarize and discuss the results.

2. Occurrence of Radial Arcs

2.1. Existence of Radial Critical Curves

Axially symmetric lenses are completely described by their surface-mass density $\Sigma(x)$ in units of a critical surface mass density $\Sigma_{\rm cr}$,

$$\kappa(x) \equiv \frac{\Sigma(x)}{\Sigma_{\rm cr}}\,, \tag{2.1}$$

where $\Sigma_{\rm cr}$ is determined by the angular-diameter distances between the observer and the lens $D_{\rm d}$, the lens and the source $D_{\rm ds}$, and the observer and the source $D_{\rm s}$,

$$\Sigma_{\rm cr} = \frac{c^2}{4\pi G}\,\frac{D_{\rm s}}{D_{\rm d}D_{\rm ds}}\,. \tag{2.2}$$

For general references on gravitational lensing, see Schneider, Ehlers, & Falco (1992) or Blandford & Narayan (1992).

The mass inside radius x is conveniently described by the dimensionless function

$$m(x) \equiv 2 \int_0^x dy\, y\kappa(y) \,. \tag{2.3}$$

Locally, the lens mapping is described by its Jacobian matrix $\mathcal{A}$, which is symmetric and thus can be diagonalized. Its two eigenvalues are

$$\lambda_\mathrm{r} = 1 - \frac{d}{dx}\,\frac{m}{x} \,, \quad \lambda_\mathrm{t} = 1 - \frac{m}{x^2} \,. \tag{2.4}$$

Radial and tangential critical curves arise if and when the conditions

$$\lambda_\mathrm{r} = 0 \,, \quad \lambda_\mathrm{t} = 0 \tag{2.5}$$

are satisfied, respectively.

The density profile (1.1) implies the surface mass density

$$\Sigma(x) = \frac{2\rho_\mathrm{s} r_\mathrm{s}}{x^2 - 1}\, f(x) \,, \tag{2.6}$$

with

$$f(x) = \begin{cases} 1 - \frac{2}{\sqrt{x^2-1}} \arctan \sqrt{\frac{x-1}{x+1}} & (x > 1) \\ 1 - \frac{2}{\sqrt{1-x^2}} \operatorname{arctanh} \sqrt{\frac{1-x}{1+x}} & (x < 1) \\ 0 & (x = 1) \end{cases} \,. \tag{2.7}$$

If we define $\kappa_\mathrm{s} \equiv \rho_\mathrm{s} r_\mathrm{s} \Sigma_\mathrm{cr}^{-1}$,

$$\kappa(x) = 2\kappa_\mathrm{s}\, \frac{f(x)}{x^2 - 1} \,, \tag{2.8}$$

and the dimensionless mass $m(x)$ becomes

$$m(x) = 4\kappa_\mathrm{s}\, g(x) \,, \tag{2.9}$$

where

$$g(x) = \ln \frac{x}{2} + \begin{cases} \frac{2}{\sqrt{x^2-1}} \arctan \sqrt{\frac{x-1}{x+1}} & (x > 1) \\ \frac{2}{\sqrt{1-x^2}} \operatorname{arctanh} \sqrt{\frac{1-x}{1+x}} & (x < 1) \\ 1 & (x = 1) \end{cases} \,. \tag{2.10}$$

It is now easy to see that

$$\begin{matrix} \frac{d}{dx}\frac{m}{x} \to \infty & (x \to 0) \\ \frac{d}{dx}\frac{m}{x} \to 0 & (x \to \infty) \end{matrix} \,. \tag{2.11}$$

Since $(d/dx)(m/x)$ is continuous, it follows from eq. (2.11) that there must be a radius x_r where $\lambda_\mathrm{r} = 0$ is satisfied, and hence the singular profile (1.1) must have a radial critical curve for any value of ρ_s and r_s. Therefore, despite of its central singularity, the density profile (1.1) can produce radial arcs. Needless to say, the profile (1.1) also always has a tangential critical curve at radius x_t. Figure 1 displays the radii x_r and x_t, the radial eigenvalue at the position of the tangential critical curve $\lambda_\mathrm{r}(x_\mathrm{t})$ and the tangential eigenvalue at the position of the radial critical curve $\lambda_\mathrm{t}(x_\mathrm{r})$ as a function of κ_s.

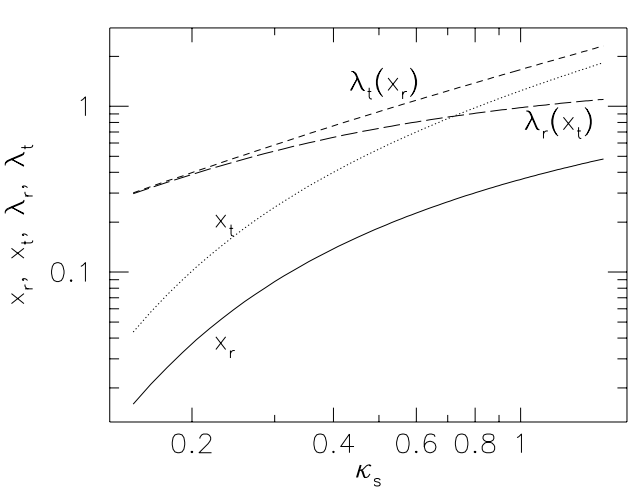

Figure 1.– Locations $x_{\rm r,t}$ of the radial and tangential critical curve (solid and dotted lines, respectively) of the density profile (1.1), and radial and tangential eigenvalues $\lambda_{\rm r}(x_{\rm t})$ and $\lambda_{\rm t}(x_{\rm r})$ at the positions of the tangential and radial critical curves (long- and short-dashed lines, respectively), all as functions of $\kappa_{\rm s}$.

2.2. Influence of External Shear

In the presence of external shear $\gamma > 0$, the eigenvalues of the Jacobian matrix of the lens mapping are changed to

$$\lambda_{\rm r} \to \lambda_{\rm r} + \gamma\cos 2\theta\ , \quad \lambda_{\rm t} \to \lambda_{\rm t} - \gamma\cos 2\theta\ , \tag{2.12}$$

where θ is the polar angle. These expressions are valid to first order in γ. Coordinates have been chosen such that the coordinate axes are the principal axes of the external shear matrix. This can be done without loss of generality because the unperturbed profile is axially symmetric.

We first note that the condition for the occurrence of a radial critical curve remains unchanged by a spatially constant external shear field for $\gamma < 1$. From the condition $\lambda_{\rm r} = 0$ and eq. (2.4), we have

$$\frac{d}{dx}\,\frac{m}{x} = 1 + \gamma\cos 2\theta\ . \tag{2.13}$$

We have seen in eq. (2.11) that the left-hand side takes any positive value, so that the presence of an external shear field $\gamma < 1$ changes the location of the radial critical curve, but cannot make it disappear.

The amount by which the critical curves are moved by the external shear field follows from

$$\Delta x = \left(\frac{d\det\mathcal{A}}{dx}\right)^{-1}\,\Delta\det\mathcal{A}\ , \tag{2.14}$$

where $\mathcal{A}$ is the Jacobian matrix of the lens mapping and $\det\mathcal{A} = \lambda_{\rm r}\lambda_{\rm t}$. To first order in γ, we find from eq. (2.12) that external shear changes $\det\mathcal{A}$ by

$$\Delta\det\mathcal{A} = \gamma\cos 2\theta\,(\lambda_{\rm t} - \lambda_{\rm r})\ , \tag{2.15}$$

and eq. (2.14) becomes

$$\Delta x = \gamma\cos 2\theta\,\frac{(\lambda_{\rm t} - \lambda_{\rm r})}{\lambda_{\rm t}'\lambda_{\rm r} + \lambda_{\rm t}\lambda_{\rm r}'}\ , \tag{2.16}$$

where primes denote the derivative with respect to x. Hence, the radial and the tangential critical curves (where $\lambda_\mathrm{r} = 0$ and $\lambda_\mathrm{t} = 0$, respectively) are shifted by

$$\Delta x_\mathrm{r} = \frac{\gamma \cos 2\theta}{\lambda_\mathrm{r}'(x_\mathrm{r})} \;, \quad \Delta x_\mathrm{t} = -\frac{\gamma \cos 2\theta}{\lambda_\mathrm{t}'(x_\mathrm{t})} \;. \tag{2.17}$$

Since the derivatives of λ_r and λ_t at the locations of the respective critical curves are of order unity (cf. Fig. 2), the shifts of the critical curves are of order of the external shear γ. We shall see later that the conclusions obtained from the radial and tangential arcs in MS 2137 and A 370 do not depend sensitively on the precise locations of the arcs. Therefore a possible shift of the critical curves by an external shear field is insignificant in the cases of these clusters. Also, the mass contributed by a central cluster galaxy can shift in particular the radial critical curve (Miralda-Escudé 1995), but it would not alter the conclusions below for the same reason as for an external shear field. I therefore neglect a possible contribution from a central galaxy altogether.

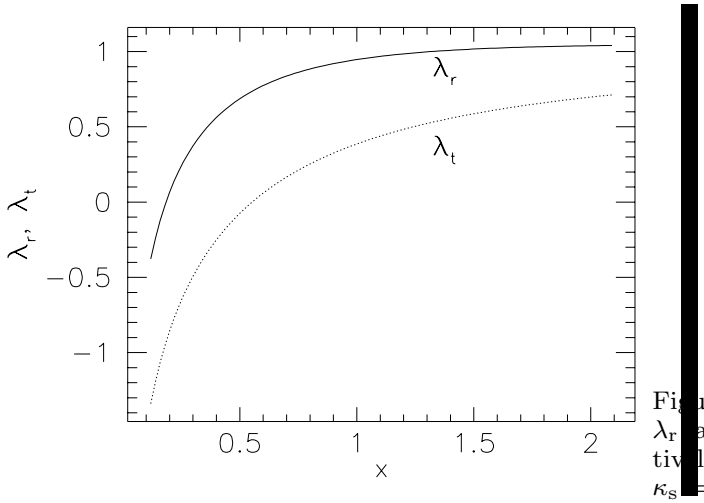

Figure 2.– Radial and tangential eigenvalues λ_r and λ_t (solid and dotted lines, respectively) as a function of radial distance x, for $\kappa_\mathrm{s} = 0.5$.

2.3. Profile Parameters from Tangential and Radial Arcs

If radial and tangential arcs appear in one cluster, we can infer the parameters r_s and ρ_s from the location of the two arcs alone.

Radial and tangential arcs appear close to the respective critical curves. Therefore their positions x_r and x_t must satisfy eq. (2.5). From eq. (2.4), we obtain for the position of the tangential arc

$$4\kappa_{\mathrm{s,t}} \frac{g(x_\mathrm{t})}{x_\mathrm{t}^2} = 1 \;, \tag{2.18}$$

and from the position of radial arc we can conclude

$$4\kappa_{\mathrm{s,r}} \left(\frac{g'(x_\mathrm{r})}{x_\mathrm{r}} - \frac{g(x_\mathrm{r})}{x_\mathrm{r}^2} \right) = 1 \;. \tag{2.19}$$

Note that the factor κ_s is generally different for the two arcs because their sources can be at different redshifts.

Combining eqs. (2.18) and (2.19), and taking eq. (2.2) into account, we have

$$\sigma \equiv \frac{\Sigma_{\rm cr,r}}{\Sigma_{\rm cr,t}} = \left(\frac{g'(\alpha x_{\rm t})}{\alpha x_{\rm t}} - \frac{g(\alpha x_{\rm t})}{(\alpha x_{\rm t})^2} \right) \frac{x_{\rm t}^2}{g(x_{\rm t})} \ , \tag{2.20}$$

where α is defined as

$$\alpha \equiv \frac{x_{\rm r}}{x_{\rm t}} \ . \tag{2.21}$$

The ratio σ between the critical surface mass densities for the radial and the tangential arc depends on the redshifts of the arcs and the cluster, and on the cosmological parameters. For definiteness, we assume an Einstein-de Sitter model universe in the following where necessary. The ratio α is observable, and so is the ratio σ, at least in principle. Given α and σ, we can solve eq. (2.20) for $x_{\rm t}$. Since we know the physical distance of the tangential arc from the cluster center $r_{\rm t}$, we can then infer the scale radius $r_{\rm s}$ of the cluster profile, and either of eqs. (2.18) and (2.19) then yields $\rho_{\rm s}$. In practice, the problem is of course that the redshifts of the arcs are difficult to measure because of their generally low surface brightness. I shall now discuss the two known cases where radial and tangential arcs have been found in galaxy clusters.

3. The Cases of MS 2137 and A 370

3.1. MS 2137

The first radial arc was detected by Fort et al. (1992) in the cluster of galaxies MS 2137, which is at redshift $z_{\rm c} = 0.315$. In the same cluster, there is an approximately tangentially oriented, giant luminous arc. The radial arc is at $r_{\rm r} = 5\farcs0$ from the cluster center, while the tangential arc is at $r_{\rm t} = 15\farcs5$. Redshift information is not available for either arc, but Mellier, Fort, & Kneib (1993) tentatively conclude from the color of the tangential arc that its redshift is $z_{\rm t} = 1.5 \pm 0.5$. Hence for MS 2137, $\alpha = 0.32$, but σ is unknown. In Fig. 3, I plot $x_{\rm t}$ as a function of σ for $\alpha = 0.32$ and for 0.75α and 1.25α.

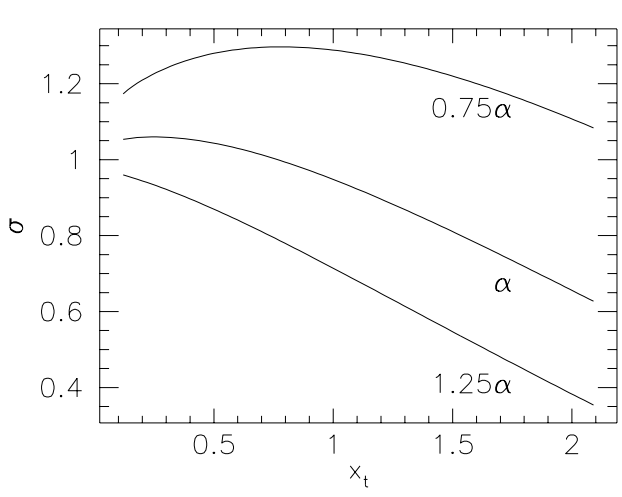

Figure 3.– σ as function of $x_{\rm t}$ for $\alpha = 0.32$ (central line) and for α lowered and increased by 25%, as indicated.

Since the redshifts of the arcs are unknown, σ is so far unconstrained, and we therefore cannot infer $r_{\rm s}$ and $\rho_{\rm s}$ for the cluster MS 2137. Numerical simulations of dark halos within the framework of the CDM cosmogony predict that $r_{\rm s}$ is approximately 20% of the tidal radius r_{200}, or on the order of $\sim 250\,h^{-1}$ kpc for a cluster-mass halo. The tangential arc in MS 2137 is at $r_{\rm t} = 15\farcs5$, or

$$r_{\rm t} = 45\,h^{-1}\ {\rm kpc} \tag{3.1}$$

at the cluster redshift. This implies $x_{\rm t} \sim 0.2$. We can read off from Fig. 3 that such low values of $x_{\rm t}$ indicate $1 \lesssim \sigma \lesssim 1.2$. To see what this means for the arc redshifts, I plot in Fig. 4 σ as a function of the radial-arc redshift $z_{\rm r}$ for five values of the tangential-arc redshift $z_{\rm t}$.

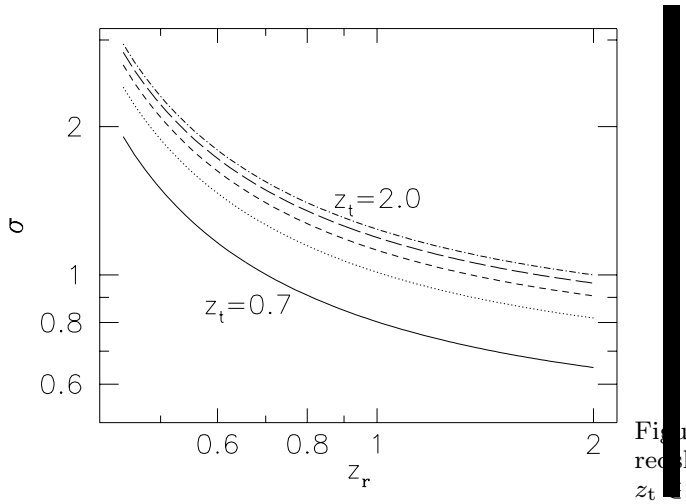

Figure 4.– σ as a function of the radial-arc redshift $z_{\rm r}$ for the five tangential-arc redshifts $z_{\rm t} \in \{0.7, 1.0, 1.4, 1.7, 2.0\}$.

The figure shows that σ is monotonically decreasing for increasing $z_{\rm r}$. By definition, it is unity if both arcs are at the same redshifts. Hence the requirement that $\sigma \simeq 1$ from above predicts that, if the cluster MS 2137 can be modeled with the density profile (1.1), the arcs either have to be at very similar redshifts, or that both have to be at much higher redshifts than the cluster, $z_{\rm r,t} \gtrsim 1$. If spectroscopy should reveal that the arcs are at discrepant redshifts, it would mean that the cluster MS 2137 cannot be modeled with the profile (1.1).

There is, however, another difficulty with $x_{\rm t}$ being so low as ~ 0.2, which can be read off from Fig. 1. Consider the radial eigenvalue $\lambda_{\rm r}(x_{\rm t})$ at the position of the tangential critical curve. The radial magnification of the tangential arc is given by the inverse of $\lambda_{\rm r}(x_{\rm t})$, which is plotted for $\kappa_{\rm s} = 0.5$ in Fig. 2. Since for $x_{\rm t} \sim 0.2$ the radial eigenvalue is $\lambda_{\rm r}(x_{\rm t}) \sim 0.5$, the tangential arc should be magnified in the radial direction by a factor of about two. Mellier et al. (1993) report that the arc seems embedded in a faint halo of width $2''$, and the main blue bright structure is marginally resolved or unresolved at a seeing of $0\farcs8$. The source should therefore have a radial width of $\lesssim 0\farcs4$, or $\lesssim 1''$ for the more extended halo. Thin tangential arcs located well within the scale radius $r_{\rm s}$ therefore require sources which are very narrow in the radial direction.

Generally, the width magnification of a tangential arc is in good approximation given by to $[2(1-\kappa(x_{\rm t}))]^{-1}$ (e.g. Hammer 1991), where $\kappa(x_{\rm t})$ is the scaled surface-mass density

at the location of the tangential arc. Statistically, cluster substructure tends to increase the separation of tangential arcs from the cluster center. Then, $\kappa(x_{\rm t})$ and therefore also the radial magnification are decreased (Bartelmann, Steinmetz, & Weiss 1995). The difficulty with the large width magnifications of tangential arcs implied by the profile (1.1) is therefore alleviated in the presence of cluster substructure.

3.2. A 370

The radial arc in Abell 370 was reported by Smail et al. (1995), while the giant tangential arc in that cluster was the first arc to be discovered (Soucail et al. 1987; Lynds & Petrosian 1989). The situation is more complicated in this cluster because it is evidently bimodal. If we assume, however, that the cluster clump where both the tangential and the radial arcs are found can be modeled with the profile (1.1), we can apply a similar analysis to that cluster also. The cluster is at redshift $z_{\rm c} = 0.375$, and the ratio between the distances of the radial and the tangential arc to the center of the subcluster where they are found is approximately $\alpha = 0.7$ (read off from Fig. 2 of Smail et al. 1995). The angular separation between the tangential arc and the subcluster center is $r_{\rm t} \simeq 10''$, or

$$r_{\rm t} \simeq 32\, h^{-1}\ {\rm kpc} \tag{3.2}$$

at the redshift of the cluster. As in Fig. 3, we plot in Fig. 5 σ as a function of $x_{\rm t}$ for α and $0.75\alpha, 1.25\alpha$.

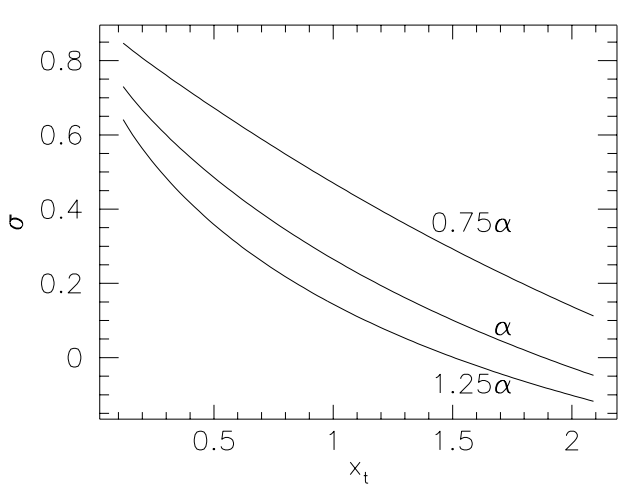

Figure 5.– σ as function of $x_{\rm t}$ for $\alpha = 0.7$ (central line) and for α lowered and increased by 25%, as indicated.

First, it is reassuring that the curves in Fig. 5 for the three values of α are not much different for $x_{\rm t} \lesssim 0.5$. We have discussed above that an external shear field γ can shift the critical curves and thus change α by an amount of order γ. Therefore, a possible shift of the critical curves by the shear field expected from the second subcluster in A 370 does not have a pronounced influence. Again, the redshift of the radial arc is unknown so that σ remains unconstrained. Assuming again the results from numerically simulated cluster-mass halos, we infer that $x_{\rm t} \simeq 0.13$, and then $0.6 \lesssim \sigma \lesssim 0.8$. From Fig. 4, we can then predict that the arc redshifts cannot be the same. Since $\sigma < 1$, the radial arc must be at a higher redshift than the tangential arc. The profile (1.1) requires the tangential arc to be

at a redshift $z_{\rm t} \lesssim 0.7$, which is in good qualitative agreement with the redshift $z_{\rm t} = 0.724$ spectroscopically determined by Soucail et al. (1988). The radial arc must then be at a very high redshift, $z_{\rm r} \sim 1.5$. Again, if the radial arc redshift should be lower than $z_{\rm r} \sim 1$, the subcluster of A 370 where the arcs are located cannot be described by the profile (1.1). From the detailed and successful lens model for A 370 by Kneib et al. (1993), Smail et al. (1995) conclude that the radial arc must be at a redshift $z_{\rm r} = 1.3 \pm 0.2$, again in qualitative agreement with the prediction above. The same difficulty with the radial magnification of the tangential arc as in MS 2137 applies here. If $x_{\rm t} \sim 0.13$ as the numerical simulations indicate, then the radial magnification should be ~ 2.5, and then the radial intrinsic source size should be $\sim 0\farcs6$. Again, cluster substructure can reduce the width of tangential arcs as discussed before.

From Fig. 1, we can read off that $x_{\rm t} \sim 0.13$ corresponds to $\kappa_{\rm s} \sim 0.2$. For the redshifts of A 370 and the tangential arc in that cluster, eq. (2.2) implies $\Sigma_{\rm cr} = 1.41\,h$ g cm^{-2}, hence $\Sigma_{\rm s} \equiv \rho_{\rm s} r_{\rm s} \sim 0.28\,h$ g cm^{-2}. With $r_{\rm s} \sim 250\,h^{-1}$ kpc, this yields for the characteristic overdensity defined by Navarro et al. (1995b)

$$\delta_{\rm c} \sim 2 \times 10^4 \tag{3.3}$$

for $\Omega_0 = 1$, corresponding to a concentration parameter (Navarro et al. 1995b) of

$$c \equiv \frac{r_{200}}{r_{\rm s}} \sim 7\,. \tag{3.4}$$

This is again in good qualitative agreement with the results from numerical simulations.

4. Summary and Conclusions

Navarro et al. (1995a,b) found that the dark-matter density profiles of halos formed in the CDM cosmogony can very well be fit with the two-parameter function (1.1) over a very wide range of halo masses. Simulations by Cole & Lacey (1995) confirm this result for a variety of power-law density perturbation spectra. Here, I have investigated whether this particular profile, which seems to be a universal function describing the structure of dark-matter halos independent of their size and environment, can account for the radial arcs observed in two clusters of galaxies despite the claim that radial arcs require non-singular, flat density profiles. I showed that the profile necessarily produces a radial critical curve for any combination of the two parameters $\rho_{\rm s}$ and $r_{\rm s}$, and that the result is robust against perturbing the potential with an external shear field $\gamma < 1$.

For clusters which produce radial and tangential arcs simultaneously, both profile parameters can be inferred if the distances of the arcs from the cluster center and their redshifts can be measured. Radial arcs have so far been reported in two clusters only, viz. MS 2137 and A 370, but some more have recently been observed. It is of potential importance for cosmological models to measure the parameters of the potential (1.1) because numerical simulations indicate that they depend on cosmological parameters.

In MS 2137, the redshifts of both arcs are unknown. Assuming scale radii on the order of $250\,h^{-1}$ kpc which are found in numerical simulations, I have shown that the

ratio between the angular separations of the radial and the tangential arc from the cluster center in MS 2137 requires them to be either at very similar redshifts, or at redshifts $\gtrsim 1$. In A 370, the same reasoning leads to the requirement that the tangential arc must be at a redshift $\lesssim 0.7$ and the radial arc at a redshift ~ 1.5 in order to reconcile their relative positions with the profile (1.1) and the numerically found scale radius. Spectroscopy (Soucail et al. 1988) reveals that the tangential arc in A 370 has a redshift of 0.724, in good qualitative agreement with the requirement found here.

There is one potential difficulty with lensing by the profile (1.1) though, because tangential arcs usually appear at distances of several 10 kpc from the cluster center, while numerical simulations yield scale radii on the order of several 100 kpc. Therefore, the tangential arcs must be formed well within the scale radius, and there their radial magnification is high, $\sim 3 \ldots 5$ for typical values. This would imply that the radial source size of the arc sources should be of order $0\farcs2 \ldots 0\farcs3$ in order to reconcile the observed tangential-arc widths with this radial magnification.

Acknowledgements. I thank Peter Schneider, Simon White, and Jordi Miralda-Escudé for useful comments. This work was supported in part by the Sonderforschungsbereich SFB 375-95 of the Deutsche Forschungsgemeinschaft.

References

Bartelmann, M., Steinmetz, M., & Weiss, A. 1995, A&A, 297, 1
Blandford, R.D., & Narayan, R. 1992, ARA&A, 30, 311
Cole, S., & Lacey, C. 1995, preprint
Fort, B., Le Fèvre, O., Hammer, F., & Cailloux, M. 1992, ApJ, 399, L125
Hammer, F. 1991, ApJ, 383, 66
Kneib, J.-P., Mellier, Y., Fort, B., & Mathez, G. 1993, A&A, 273, 367
Lynds, R., & Petrosian, V. 1989, ApJ, 336, 1
Mellier, Y., Fort, B., & Kneib, J.-P. 1993, ApJ, 407, 33
Miralda-Escudé, J. 1993, ApJ, 403, 497
Miralda-Escudé, J. 1995, ApJ, 438, 514
Navarro, J., Frenk, C.S., & White, S.D.M. 1995a, MNRAS, 275, 720
Navarro, J., Frenk, C.S., & White, S.D.M. 1995b, MNRAS, in press
Schneider, P., Ehlers, J., & Falco, E.E. 1992, Gravitational Lenses (Heidelberg: Springer)
Smail, I., Dressler, A., Kneib, J.-P., Ellis, R.S., Couch, W.J., Sharples, R.M., & Oemler, A. 1995, SISSA preprint 9503063
Soucail, G., Fort, B., Mellier, Y., & Picat, J.P. 1987, A&A, 172, L14
Soucail, G., Mellier, Y., Fort, B., Mathez, G., & Cailloux, M. 1988, A&A, 191, L19